Pharmacogenomic Identification of Targets for Adjuvant Therapy with the Topoisomerase Poison Camptothecin

Jonathan P. Carson, Nianyi Zhang, Garrett M. Frampton, Norman P. Gerry, Marc E. Lenburg, and Michael F. Christman

Department of Genetics and Genomics, Boston University School of Medicine, Boston, Massachusetts

ABSTRACT

The response of tumor cells to the unusual form of DNA damage caused by topoisomerase poisons such as camptothecin (CPT) is poorly understood, and knowledge regarding which drugs can be effectively combined with CPT is lacking. To better understand the response of tumor cells to CPT and to identify potential targets for adjuvant therapy, we examined global changes in mRNA abundance in HeLa cells after CPT treatment using Affymetrix U133A GeneChips, which include all annotated human genes (22,283 probe sets). Statistical analysis of the data using a Bayesian/Cyber t test and a modified Benjamini and Hochberg correction for multiple hypotheses testing identified 188 probe sets that are induced and 495 that are repressed 8 h after CPT treatment at a False Discovery Rate of <0.05 and a minimum 3-fold change. This pharmacogenomic approach led us to identify two pathways that are CPT induced: (*a*) the epidermal growth factor receptor; and (*b*) nuclear factor-κB-regulated antiapoptotic factors. Experiments using HeLa cells in our lab and prior animal model studies performed elsewhere confirm that inhibitors of these respective pathways super-additively enhance CPT's cytotoxicity, suggesting their potential as targets for adjuvant therapy with CPT.

INTRODUCTION

The ability to induce apoptosis in tumor cells is critical to elicit a positive response to cytotoxic chemotherapy (1). In recent years, the characterization of the complete human transcriptome has enabled investigators to observe the changes in gene expression that accompany programmed cell death induced by diverse insults. This molecular profiling of gene expression from tumor biopsies has begun to yield diagnostic and prognostic information of unprecedented accuracy (2).

Camptothecin (CPT) is a plant alkaloid derived from the tree, *Camptotheca acuminata*. Its derivatives have shown promise in clinical trials for use against small cell lung carcinoma (3) and other malignancies, including cervical cancer (4). The compound exhibits high specificity for topoisomerase I (topo I), which it inhibits by preventing the religation step of this enzyme's DNA relaxing activity. In the presence of CPT, topo I forms a covalent intermediate with the 3′-phosphate end of the broken DNA strand (5). This single-strand nick lesion is believed to convert into an irreversible double-strand break after it encounters the replication fork machinery in S phase. This unusual form of DNA damage induces a signaling cascade that is propagated by ATM-family kinases in human cells (6), which phosphorylate numerous targets involved in transcription, DNA repair, cell cycle arrest, and apoptosis.

A comprehensive survey of the entire transcriptome after CPT treatment via the Affymetrix U133A Chip has not been reported, although one study examined a small number of genes after CPT

Requests for reprints: Michael F. Christman. Phone: (617) 414-1636; Fax: (617) 414-1646; E-mail: mfc@bu.edu; Internet address: http://www.gg.bu.edu.

treatment (7). Moreover, it remains unclear whether such information could be of therapeutic value. In the following study, we present data generated using the Affymetrix U133A chip (22,283 probe sets) from total RNA collected from HeLa cells treated with CPT at a dose (10 μM) and time (8 h) sufficient to induce rapid apoptosis. We observed significant 3-fold changes in expression of 683 genes, including novel transcripts and several putative p53-regulated genes. Consistent with the induction of certain p53-responsive genes, we observed increased protein levels of p53, phosphorylation on serine 15, and S-phase arrest after CPT treatment. Moreover, we detected striking evidence of nuclear factor (NF)-κB transactivation and epidermal growth factor receptor (EGFR) survival signaling (via HB-EGF). We reasoned that changes in the gene expression pattern might represent regulation of pathways important for CPT survival. The data were used to generate the hypothesis that inhibition of the NF-κB and EGFR pathways would increase the sensitivity of HeLa cells to CPT. Administration of an inhibitor of this pathway, AG1478, yielded a superadditive increase in apoptosis when administered in combinations with CPT. Inhibition of NF-κB signaling has been shown to dramatically increase tumor cell sensitivity to CPT-11 (8, 9). These results suggest both that CPT may be effective in mobilizing a p53 response in cervical carcinomas and that data from microarray experiments can form the basis for rational hypotheses in the treatment of cancer.

MATERIALS AND METHODS

RNA Isolation. Total RNA was extracted from HeLa cells plated 24 h previously at a density of ~40,000 cells/cm² (~75% confluence) using an RNAeasy mini-kit (Qiagen, Valencia, CA).

Chemicals. All chemicals and reagents, unless otherwise specified, were purchased from Sigma-Aldrich (St. Louis, MO).

Cell Culture. HeLa cells were purchased from the American Type Culture Collection (Manassas, VA) and maintained at 37°C in 5% CO_2 in DMEM (Mediatech, Herndon, VA) containing 10% fetal bovine serum supplemented with penicillin/streptomycin (Hyclone, Logan, UT). Experiments listed here were conducted on cells that had been passaged three to seven times following arrival from American Type Culture Collection.

Apoptosis Response and p53 Activation. HeLa cells were plated at a density of 10^6 cells/6 cm-diameter tissue culture dish and incubated 16 h. Culture medium was then removed and replaced with media containing varying doses of CPT and/or inhibitors. At times of data collection, both floating (apoptotic and/or necrotic cells) and adherent cell material from each dish were collected on ice using cell lifters and centrifugation (5 min × 200 g). Next, cell pellets were resuspended in ice-cold PBS, centrifuged again (5 min × 200 g), and lysed in 200 μl of lysis buffer [1% Igepal, 0.5% deoxycholate, 2 mM DTT, 150 mM NaCl, and 20 mM HEPES (pH 7.4); supplemented with phosphatase and protease inhibitors]. Protein concentrations in lysates were determined by the Bio-Rad assay, and 100 μg/lane samples were immediately prepared for loading onto 12% acrylamide SDS-PAGE by boiling (5 min) in 1% SDS sample buffer. Completed gels were then electrotransferred to nitrocellulose membranes, which were stained with Ponceau S and cut in half across protein bands corresponding to ~M_r 35,000. Membrane halves corresponding to higher molecular weight proteins were Western blotted with primary antibodies directed against whole p53 protein (Ab-12; Oncogene Research Products, San Diego, CA) and serine-15-phosphorylated p53 (Cell Signaling Technology, Beverly, MA); membranes corresponding to the lower molecular weight proteins were Western blotted with an antibody directed against the M_r 23,000

caspase-specific cleavage product of poly(ADP-ribose) polymerase (R&D Systems, Minneapolis, MN). These Western blot procedures were conducted according to the directions of the manufacturer, and immunoreactive bands were visualized by chemiluminescent exposure to instant film such that sub-saturation exposures ($\sim$1 min) were obtained. These film images were then digitally scanned and converted to .tiff images by Adobe PhotoShop with the "Autolevels" (Shft+Ctrl+L) image function selected.

Scanned Western blot images were then analyzed with the Scion Image software package freely available from ScionCorp.[1] The immunoreactive bands were highlighted, and pixel counts of each band were obtained via the Integrated Density analysis option. Integrated densities were linearly normalized such that the gel band corresponding to the positive control in the experiment (10 μM CPT at 8 h.) was assigned an immunoreactivity value of 100.

WST-1 Viability Assay. HeLa cells were plated at a density of 10,000 cells/well on a 96-well tissue culture plate. Twenty-four h later, media (DMEM +10% FCS) containing varying concentrations of CPT +/− AG1478 (500 nM) were added. Twelve h later, 10 μl/well of the viability stain, WST-1 (Roche Biochemicals, Indianapolis, IN), were added for 30 min. Colorimetric readings were obtained by plate reader at 450 nm. The average of data points from wells containing WST-1-stained media, alone (with no cells), was subtracted from the raw data from wells containing cells. Percent decline in viability/well was calculated as

$$\frac{(A_{450\ nm} \text{ in treated well}) - (\text{average } A_{450\ nm} \text{ in untreated, negative control wells}) \times 100}{(\text{average } A_{450\ nm} \text{ in untreated, negative control wells})}$$

RNA Labeling and Hybridization. Using a poly-dT primer incorporating a T7 promoter, double-stranded cDNA was synthesized from 10 μg of total RNA using a Superscript cDNA Synthesis kit (Invitrogen, Carlsbad, CA). Double-stranded cDNA was purified by phenol/chloroform extraction. The aqueous phase was isolated using Phase-Lock Gel Heavy (Brinkmann Instruments, Westbury, NY) and the cDNA ethanol precipitated. Subsequently, biotin-labeled cRNA was generated from the double-stranded cDNA template though *in vitro* transcription with T7 polymerase using a BioArray High Yield RNA Transcript Labeling kit (Enzo Diagnostics, Farmingdale, NY). The biotinylated cRNA was purified using RNeasy affinity columns (Qiagen). Biotinylated cRNA (20 μg) was fragmented in 40 mM Tris-acetate (pH 8.1), 100 mM KOAc, and 30 mM MgOAc for 35 min at 94°C to an average size of 35–200 bases. Fragmented, biotinylated cRNA (10 μg), along with hybridization controls (Affymetrix, Santa Clara, CA), were hybridized to Affymetrix Human Genome U133A GeneChip arrays containing probes for 22,283 transcripts. The arrays were hybridized for 16 h at 45°C and 60 rpm. After hybridization, arrays were washed and stained according to the standard Antibody Amplification for Eukaryotic Targets protocol (Affymetrix). The stained GeneChip arrays were scanned at 488 nm using a G2500AGeneArray Scanner (Agilent, Palo Alto, CA) and Microarray Suite 5.0 software (Affymetrix).

Data Quantification and Normalization. After data acquisition, the scanned images were quantified using Microarray Suite 5.0 software (Affymetrix) yielding a signal intensity for each probe on the GeneChip. The signal intensities from the 22 probes for each gene were then used to determine an overall expression level according to algorithms implemented in Microarray Suite 5.0. The arrays were then linearly scaled to an average expression level of 500 units on each chip. Scaling factors varied from 2.29 to 4.30. Upon publication, complete microarray data for each sample will be made publicly available through National Center for Biotechnology Information's Gene Expression Omnibus.[2]

RESULTS

Gene Expression Changes Induced by CPT. HeLa cells grown to 75% confluence were treated with 10 μM CPT or a solvent control (DMSO) for 8 h. After isolation of total RNA, cDNAs and cRNAs were generated and hybridized to U133A GeneChips as per a standard protocol (Affymetrix). This procedure was repeated four times on separate occasions; one CPT-treated sample failed to hybridize. Gene expression changes between the three CPT-treated samples and four untreated samples were then tabulated and analyzed after normalization ("Materials and Methods").

Data Analysis. For each gene, fold-change (FC) and statistical significance of differential expression (*p*) were calculated. FC was calculated using the average signal from the two groups. Statistical significance was calculated using a *t*-Test implemented in Cyber-T.[3] Cyber-T uses a Bayesian estimate of the variance within treatment groups based on a prior distribution obtained from an estimate of the variance from genes at a similar expression level. This provides increased power to identify differentially expressed genes because the variability within groups is estimated based on a larger number of data points.

To correct significance estimates for multiple hypothesis testing we used a modified version the false discovery rate (FDR) method of Benjamini and Hochberg (10), which calculates a new test statistic that estimates the portion of type I errors within a group of genes meeting a significance cutoff. This modified FDR is the quotient of the number of unchanged genes expected at a given significance cutoff over the number of genes detected at that significance cutoff.

$$FDR = \frac{\text{number of false positives expected}}{\text{number of genes detected at a given level of significance}}$$

Two assumptions—that changed genes would not have $p > 0.90$ and that unchanged genes would have an even distribution of Ps between 0 and 1—were used to estimate the number of unchanged genes. A total of 1,412 genes had $p > 0.90$; thus, it was estimated that 14,120 genes were not differentially expressed between the treatment groups. Because we have assumed that these unchanged genes will have an even distribution of *p* values, $p * 14{,}120$ genes that were not truly differentially expressed can be expected to meet a significance cutoff *p* by chance alone. Using this model of type I errors, the set of FDRs associated with each gene was calculated as:

$$FDR = \frac{p \times 14{,}120}{\text{number of genes detected at significance level } p}$$

The FDR of a gene was then defined as the minimal FDR at which time the gene appears significant.

To define a set of differentially expressed genes, we imposed cutoffs based on statistical significance and FC. Probe sets with FDR < 0.05 were sufficiently reproducible to indicate differential expression (of any magnitude). These probe sets can be expected to have a type I (false positive) error rate of 5%. A total of 2991 probe sets were identified at FDR < 0.05, indicating that we expect $\sim$2840 of these genes to in fact be differentially expressed. Genes with FC > 3 were considered sufficiently changed to indicate biological meaning. A total of 1009 genes, the expression of which was 3-fold changed as a result of CPT treatment, was detected. The criterion for biological significance, a change of ≥3-fold, is clearly somewhat arbitrary and results in the exclusion of many genes meeting the significance threshold from additional analysis. Combining the FC a significance cutoffs, we generated a list of 188 genes, the expression of which was reproducibly (FDR < 0.05) up-regulated ≥3-fold, and 495 genes, the expression of which was reproducibly down-regulated ≥3-fold.

Each gene was annotated based on a complete download of the

Table 1 *Differentially expressed genes following camptothecin treatment of HeLa cells*

A. Largest fold increases			B. Largest fold decreases			C. Most significant changes			D. Genes of unknown function		
Gene symbol	False discovery rate	Fold Change	Gene symbol	False discovery rate	Fold Change	Gene symbol	False discovery rate	Fold Change	Gene symbol	False discovery rate	Fold Change
CCL20	1.39×10^{-3}	17.9	SCA1	4.02×10^{-5}	−35.1	IER5	1.48×10^{-8}	6.2	Hypothetical protein EUROIMAGE 511235	6.95×10^{-8}	6.2
MAFF	6.95×10^{-8}	17.4	KIAA0993	6.46×10^{-5}	−26.1	SAT	4.68×10^{-8}	7.5	Hypothetical protein dJ465N24.2.1	1.21×10^{-6}	4.9
ABCF2	3.76×10^{-5}	15.2	C18orf1	8.42×10^{-4}	−25.7	TUBB	6.95×10^{-8}	5.2	Hypothetical protein FLJ10587	1.31×10^{-6}	3.6
STX11	8.44×10^{-4}	13.9	APBB2	2.27×10^{-4}	−22.7	LOC56906	6.95×10^{-8}	6.2	hbc647 mRNA sequence	2.37×10^{-6}	3.3
IL8	2.65×10^{-3}	11.0	MNAT1	1.02×10^{-4}	−20.7	ATF3	6.95×10^{-8}	6.6	Hypothetical protein dJ465N24.2.1	2.48×10^{-6}	7.1
HIS1	6.95×10^{-8}	9.9	PBX1	4.33×10^{-3}	−20.6	DKK1	6.95×10^{-8}	6.6	Hypothetical protein FLJ21870	3.16×10^{-6}	3.3
GBX2	1.90×10^{-5}	9.8	GPHN	6.17×10^{-3}	−17.5	DTR	6.95×10^{-8}	8.0	DKFZP564M182 protein	4.31×10^{-6}	3.6
FLJ22059	1.74×10^{-5}	9.8	KIAA0854	1.83×10^{-4}	−17.3	HIS1	6.95×10^{-8}	9.9	Chromosome 15 open reading frame 12	6.75×10^{-6}	2.7
HOXA11	3.43×10^{-5}	9.5	PRO1635	4.52×10^{-5}	−16.1	MAFF	6.95×10^{-8}	17.4	Hypothetical protein FLJ14547	6.84×10^{-6}	3.6
SPRY2	3.62×10^{-5}	9.0	KIAA0440	2.06×10^{-5}	−15.4	MACMARCKS	1.05×10^{-7}	4.0	Hypothetical protein MGC14376	7.56×10^{-6}	3.2
SAT	2.37×10^{-6}	8.9	RNGTT	9.81×10^{-5}	−14.4	TSSC3	1.95×10^{-7}	3.6	KIAA0110 protein	1.25×10^{-5}	2.9
APOE	5.44×10^{-4}	8.5	KIAA1025	5.32×10^{-4}	−13.3	PMAIP1	2.63×10^{-7}	3.9	Hypothetical protein FLJ38984	1.32×10^{-5}	3.0
DTR	6.95×10^{-8}	8.0	ITSN1	4.35×10^{-5}	−13.3	RIS1	4.75×10^{-7}	4.0	Hypothetical protein MGC11308	1.63×10^{-5}	3.1
SAT	4.68×10^{-8}	7.5	FLJ14115	4.75×10^{-5}	−13.2	NMA	4.94×10^{-7}	5.0	Hypothetical protein FLJ22059	1.74×10^{-5}	9.8
NSPC1	4.45×10^{-4}	7.4	XRCC4	1.36×10^{-5}	−12.4	DTR	4.94×10^{-7}	5.6	KIAA0440 protein	2.06×10^{-5}	−15.4
HSU53209	1.52×10^{-3}	7.2	BHC80	6.97×10^{-5}	−12.1	PMAIP1	7.40×10^{-7}	4.8	KIAA0903 protein	2.06×10^{-5}	−10.8
DJ465N24.2.1	2.48×10^{-6}	7.1	KIAA0769	6.25×10^{-4}	−12.0	DJ465N24.2.1	1.21×10^{-6}	4.9	Hypothetical protein FLJ12484	3.72×10^{-5}	3.1
LHX6	1.33×10^{-4}	6.7	VAV3	1.72×10^{-3}	−11.2	FLJ10587	1.31×10^{-6}	3.6	DKFZP564M182 protein	3.79×10^{-5}	4.0
DKK1	6.95×10^{-8}	6.6	CRSP8	1.08×10^{-4}	−11.1	HEAB	1.85×10^{-6}	3.8	Chromosome 5 open reading frame 6	4.00×10^{-5}	2.7
ATF3	6.95×10^{-8}	6.6	KIAA0903	2.06×10^{-5}	−10.8	GADD45A	1.85×10^{-6}	5.0	Hypothetical protein FLJ20257	4.35×10^{-5}	2.6
SAT	2.95×10^{-6}	6.4	FLJ13114	1.72×10^{-3}	−10.6	PTGER4	1.88×10^{-6}	5.7	Hypothetical protein PRO1635	4.52×10^{-5}	−16.1
HIS1	2.00×10^{-4}	6.4	GPRK5	7.40×10^{-5}	−10.3	hbc647	2.37×10^{-6}	3.3	cDNA FLJ14115 fis	4.75×10^{-5}	−13.2
IER5	1.48×10^{-8}	6.2	STK3	7.39×10^{-4}	−10.2	GADD45B	2.37×10^{-6}	6.1	Hypothetical protein MGC4504	4.75×10^{-5}	4.3
LOC56906	6.95×10^{-8}	6.2	SCA1	9.76×10^{-3}	−10.1	SAT	2.37×10^{-6}	8.9	Hypothetical protein p5326	5.35×10^{-5}	3.2
GADD45B	2.37×10^{-6}	6.1	MGC24039	3.54×10^{-3}	−10.1	DJ465N24.2.1	2.48×10^{-6}	7.1	cDNA FLJ11796 fis	5.38×10^{-5}	2.8
RFPL3S	8.42×10^{-3}	6.1	KIAA0819	5.81×10^{-4}	−10.0	H3F3B	2.49×10^{-6}	4.5	cDNA DKFZp686D0521	5.39×10^{-5}	−3.7
CLN8	3.75×10^{-3}	5.9	TBL1X	9.59×10^{-5}	−9.5	TPBG	2.82×10^{-6}	3.1	KIAA0970 protein	5.54×10^{-5}	−3.6
DUSP6	6.03×10^{-5}	5.9	MAD1L1	3.35×10^{-5}	−9.5	OSR2	2.95×10^{-6}	5.7	Hypothetical protein MGC2217	5.54×10^{-5}	3.2
EDN1	1.37×10^{-5}	5.7	NRP1	2.24×10^{-4}	−9.5	SAT	2.95×10^{-6}	6.4	KIAA0993 protein	6.46×10^{-5}	−26.1
OSR2	2.95×10^{-6}	5.7	SYNE-1	8.86×10^{-3}	−9.4	FLJ21870	3.16×10^{-6}	3.3	KIAA1102 protein	6.75×10^{-5}	−3.4
ENC1	2.31×10^{-4}	5.7	PDZD2	7.48×10^{-3}	−9.4	RBMS1	3.46×10^{-6}	−6.7	Hypothetical protein FLJ10517	6.75×10^{-5}	−3.0
PTGER4	1.88×10^{-6}	5.7	ROR2	1.54×10^{-3}	−9.2	AMACR	3.46×10^{-6}	5.1	Hypothetical protein FLJ12827	7.08×10^{-5}	2.8
H2AFJ	3.67×10^{-5}	5.6	TEM6	1.08×10^{-5}	−9.2	MYO10	3.46×10^{-6}	−4.9	Hypothetical protein FLJ10233	7.18×10^{-5}	−4.8
DTR	4.94×10^{-7}	5.6	FUT8	9.94×10^{-4}	−9.2	DKFZP564M182	4.31×10^{-6}	3.6	KIAA0182 protein	7.35×10^{-5}	−7.6
PI3	6.75×10^{-5}	5.6	PP3781	4.23×10^{-4}	−9.1	SE20-4	6.20×10^{-6}	3.6	cDNA DKFZp761P0818	7.40×10^{-5}	−3.8
THBD	2.77×10^{-4}	5.5	MAP2K5	1.74×10^{-3}	−9.1	SAS10	6.26×10^{-6}	3.6	Hypothetical protein FLJ14547	7.40×10^{-5}	2.3
SIRT4	8.19×10^{-3}	5.4	PARD3	1.64×10^{-3}	−9.0	C15orf12	6.75×10^{-6}	2.7	Hypothetical protein DKFZp564O0523	7.96×10^{-5}	3.8
ZF5128	7.64×10^{-3}	5.4	NRF1	1.05×10^{-3}	−9.0	MELK	6.84×10^{-6}	−3.9	DKFZP434C212 protein	8.49×10^{-5}	−3.6
SSI-1	2.21×10^{-3}	5.4	MPHOSPH9	2.55×10^{-4}	−8.9	FLJ14547	6.84×10^{-6}	3.6	Chromosome 1 open reading frame 28	9.24×10^{-5}	−5.2
KIAA0014	2.77×10^{-4}	5.3	MBLL39	5.16×10^{-5}	−8.8	RBMS1	7.05×10^{-6}	−5.2	Chromosome 10 open reading frame 2	1.01×10^{-4}	3.2
HOXC13	1.36×10^{-5}	5.3	RB1	5.55×10^{-4}	−8.7	TNFAIP6	7.05×10^{-6}	4.6	Hypothetical protein FLJ10697	1.02×10^{-4}	−4.4
TUBB	6.95×10^{-8}	5.2	KIAA0440	7.45×10^{-4}	−8.7	PTPRK	7.56×10^{-6}	−4.6	KIAA0469 gene product	1.02×10^{-4}	2.7
AMACR	3.46×10^{-6}	5.1	SYNJ2	2.37×10^{-4}	−8.7	TBCC	7.56×10^{-6}	3.1	PKC-α mRNA, partial 3' UTR	1.06×10^{-4}	−7.5
H3FL	7.71×10^{-4}	5.1	NVL	2.39×10^{-4}	−8.7	MGC14376	7.56×10^{-6}	3.2	KIAA1243 protein	1.12×10^{-4}	−3.7
GADD45A	1.85×10^{-6}	5.0	TNRC15	1.32×10^{-4}	−8.6	RBMS1	7.86×10^{-6}	−6.1	Hypothetical protein FLJ20752	1.16×10^{-4}	2.4
BAT1	1.11×10^{-3}	5.0	LIMK1	5.58×10^{-3}	−8.5	STC2	8.12×10^{-6}	4.0	cDNA FLJ11904 fis	1.16×10^{-4}	2.6
NMA	4.94×10^{-7}	5.0	TLK1	2.67×10^{-3}	−8.4	SDC4	8.31×10^{-6}	3.2	Hypothetical protein MGC4701	1.23×10^{-4}	2.9
DJ465N24.2.1	1.21×10^{-6}	4.9	C4ST	2.59×10^{-4}	−8.2	ENC1	8.31×10^{-6}	4.9	Hypothetical protein MGC3032	1.23×10^{-4}	2.6
FZD7	6.38×10^{-5}	4.9	PLD1	6.41×10^{-3}	−8.1	PPIF	8.81×10^{-6}	3.0	Hypothetical protein FLJ23399	1.26×10^{-4}	−6.6
TRO	9.05×10^{-2}	4.9	GW112	2.01×10^{-1}	−8.0	TACSTD2	9.79×10^{-6}	2.9	ESTs, moderately similar to CRL2	1.26×10^{-4}	6.3

NetAffx database (Affymetrix; database build date March 1, 2003). The relationship among Affymetrix Gene ID numbers and other gene descriptors such as gene symbols, Unigene clusters, GenBank designations, and so on, is summarized in Table 2*A* for clarity. We will discuss each unique Affymetrix probe set as if it were a separate gene although it is possible that two probe sets could detect different splice variant RNAs transcribed from a single Unigene cluster.

The top 50 CPT-responsive genes are displayed in rank order by greatest fold-increase (Table 1*A*), greatest fold-decrease (Table 1*B*) and greatest significance (Table 1*C*). Additionally, 170 probe sets (44 increases and 126 decreases) representing unannotated genes were identified, and 50 of these are displayed in rank order of greatest significance (Table 1*D*).

Pathways Altered by CPT Treatment. We further analyzed the 188 probe sets that were significantly induced by CPT (red box in Fig. 1*A*) and the 495 probe sets whose expression was significantly decreased by CPT exposure (green box in Fig. 1*A*) for alterations in gene expression of specific pathways and compared the results to other reports of DNA damage-inducible gene expression. Automated anal-

ysis of the genes determined to be differentially expressed was performed using the online software tool E.A.S.E.[4] E.A.S.E. identifies gene descriptors from a variety of online databases [Gene Ontology, Kyoto Encyclopedia of Genes and Genomes, Protein Families Database (Pfam), and so on] that are overrepresented within a list of genes.

NF-κB-Regulated Genes. Because the list of CPT-induced genes included many cytokines and chemokines, we examined whether genes involved in inflammation were overrepresented among CPT-induced changes. We examined the Proteome Bioknowledge Library (Incyte, Santa Clara, CA) for 169 probe sets corresponding to genes annotated with the designation Inflammatory Response (Gene Ontology term: 6954) and compared this with the list of all probe sets. (For this query—and in the other preliminary data mining examples listed in Table 2*B*—we used alternative selection criteria to FDR for determination of "changed" genes, where our significance cutoff was instead $p < 0.01$, FC > 3.0.) We found that 8.9% of inflammation
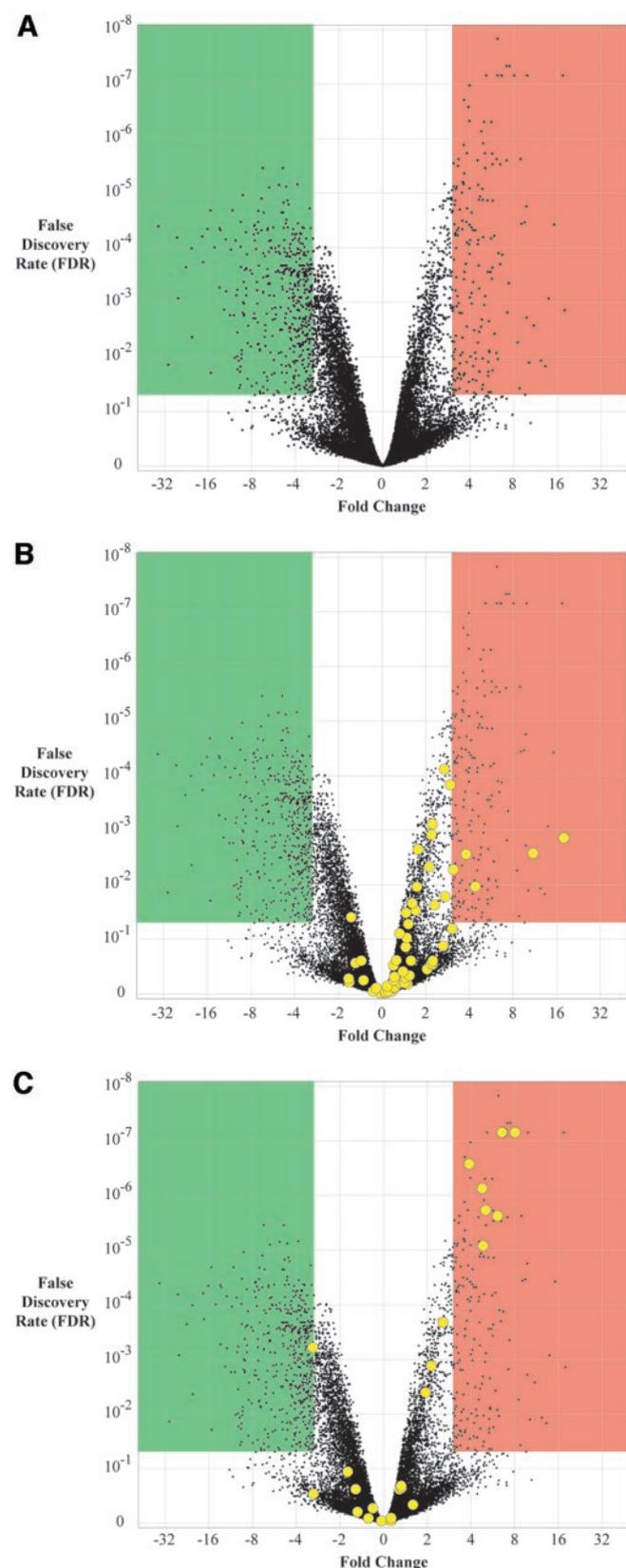

2098

Fig. 1. Fold-change (FC) and statistical significance of differential expression as a volcano scatterplot. Each transcript measured via microarray is represented by a point showing the FC and false discovery rate (FDR) measured for that transcript. FC and FDR cutoffs that define sets of up-regulated and down-regulated genes are represented by *red* and *green shaded areas*. *A*, a total of 22,283 transcripts plotted, 188 up-regulated, and 495 down-regulated. *B*, fifty-six NF-κB genes highlighted in *yellow* showing overall up-regulation compared with the entire data set. *C*, twenty-seven p53 regulated genes highlighted in *yellow* showing overall differential expression compared with the entire data set.

genes were changed after CPT treatment compared with 3.3% of all genes, a 2.7-fold overrepresentation (Table 2*B*).

Given our data suggesting that CPT treatment may induce genes involved in inflammation, we examined whether NF-κB-mediated transcription might be responsible because this factor comprises a central node in cellular responses to both inflammation and DNA damage. We analyzed a list of 56 putative NF-κB-responsive genes (11) and determined whether CPT-induced changes in expression were observed among the corresponding probe sets. This list of NF-κB-inducible genes was disproportionately changed (3.8-fold overrepresentation; Tables 2*B* and 3*A*) and up-regulated in comparison with the total list of probe sets (yellow dots in Fig. 1*B*; Table 3*A*). Moreover, a Student's *t*-Test comparison ($p = 4.1 \times 10^{-5}$) between the group of all probe set FCs ($n = 22,283$, mean FC $= -0.0$), and our list of NF-κB annotated probe set FCs ($n = 56$, mean FC $= 1.7$) strongly suggested an overall positive directionality in NF-κB-regulated gene levels. Thus, within 8 h, CPT treatment engages an NF-κB-regulated transcriptional network. The importance of the NF-κB pathway in mediating CPT-resistance has been noted (8, 9, 11); see "Discussion").

DNA Double-Strand Break Repair and Chromatin. CPT induces double-strand breakage, and we expected induction of this type of DNA damage to promote expression of specific double-strand break repair pathway genes. Surprisingly, of the 25 probe sets corresponding to genes annotated under "Biological Process: Double-Strand Break Repair" (Gene Ontology term: 6302), more were decreased in expression (Table 2*B*). One exception in this compilation was *Mre11A*, which was reported to increase in expression 2.5-fold. In addition, histone genes, as a group, were elevated in comparison with the total list of probe sets after CPT treatment (Table 2*B*). Prominent on this list were so-called variant histone genes, including *H2AFJ*, *H2BFN*, *H2BFQ*, *H3F3B*, and *H2AFN*. This suggests that the CPT-induced histone transcriptional response may involve modifications to chromatin that may facilitate repair (12).

p53-Regulated Genes. The duration (8 h) and dosage (10 μM) of CPT treatment were sufficient to induce poly(ADP-ribose) polymerase cleavage, an early marker of apoptosis, among the HeLa cell samples (Fig. 2*A*). Because apoptosis induced by DNA damaging agents is largely p53 dependent (13, 14), we asked whether a p53 response was mobilized in HeLa cells where p53 function is generally considered to be abolished by association with human papillomavirus type E6 (15). We detected dramatically increased phosphorylation of p53 on serine 15 after CPT treatment (Fig. 2*B*), as well as higher protein level (data not shown), indicating that topo I blockage in HeLa cells results in greater p53 transactivation and increased protein stability. To determine whether CPT treatment influences expression of putative p53-responsive genes, we examined a list of 31 genes that are regulated by p53 and queried their expression status among the Affymetrix probe sets. Gene expression changes in this list were, overall, positive compared with the total list of probe sets (Table 2*B*, Fig. 1*C*). Moreover, several of these genes were among the highest-fold induced probe sets such as *DTR*, *DKK1*, *ATF3*, and *GADD45* (Table 3*B*). Therefore, it is likely that CPT treatment induces a partial or cell-specific p53 response in HeLa.

Defining Potential Targets for Adjuvant Therapy with CPT. CPT treatment increases expression of several gene products involved in biochemical pathways that have been targeted in proposed clinical trials. We hypothesized that circumvention of these pathways might enhance CPT-mediated cytotoxicity. These pathways include the EGFR (16), polyamine biosynthesis (17), mitogen-activated protein kinase (18), NF-κB (8), Bcl-2 family (19–21), and histone deacetylation (22). Specifically, we report increased expression of the gene encoding HB-EGF (DTR), which is an EGFR ligand and a survival factor for HeLa cells.

Table 2 *Global response of annotated genes to camptothecin*

A. Annotation of differently expressed genes			
	Unique	Duplicate	No entry
All Genes			
Affymetrix ID	683	0	0
Gene symbol	522	109	52
GenBank	647	36	0
Unigene	560	113	10
LocusLink	522	109	52
SwissProt	521	111	51
OMIM	209	19	455
Up Genes			
Affymetrix ID	188	0	0
Gene symbol	151	22	15
GenBank	183	5	0
Unigene	161	22	5
LocusLink	151	22	15
SwissProt	144	22	22
OMIM	68	7	113
Down Genes			
Affymetrix ID	495	0	0
Gene symbol	371	87	37
GenBank	464	31	0
Unigene	399	91	5
LocusLink	371	87	37
SwissProt	377	89	29
OMIM	141	12	342

B. Biological trends in groups of annotated genes				
Annotation	# Probesets	# Up	# Down	% Changed	Mean Fold Change
All probe sets	22285	212	525	3.3%	−0.02
Nuclear compartment (GO:5634)	334	10	45	16.5%	−1.30
Proteome: DNA binding	980	11	40	5.2%	−0.13
Oncogenesis (GO:7048)	552	7	29	6.5%	−0.27
Inflammatory response (GO:6954)	169	11	4	8.9%	0.70
Biological process (GO) "Cell Cycle"	366	6	19	6.8%	−0.27
Mitosis (GO:7067, GO:7088, GO:7096)	72	1	6	9.7%	−1.11
Double-strand break repair (GO:6302)	25	0	1	4.0%	−1.40
Histone	87	6	1	8.1%	1.02
p53-inducible genes	31	8	1	28.1%	1.52
NF-κB-inducible genes	56	7	0	12.5%	1.72

The highly specific EGF receptor inhibitor, AG1478 (23, 24), is known to inhibit ATP binding to EGFR and is sufficient to abolish the antiapoptotic effect of HB-EGF at a concentration of 500 nM in HeLa (data not shown). At this concentration, AG1478 exerts an apparent superadditive effect on apoptosis together with CPT (Fig. 3*A*), where the mean immunoreactivity of M_r 23,000 cleaved poly(ADP-ribose) polymerase product from all hypothetical sums of CPT-only and AG1478-only treated samples ($n = 9$, 109.1) is significantly different (*t*-Test, $p = 1.9 \times 10^{-5}$) from the immunoreactive signal generated from cells treated with the actual combination ($n = 3$, 246.1). Moreover, AG1478 enhances viability loss over a range of CPT doses (Fig. 3, *B* and *C*). The combinatorial effects shown in Fig. 3 are consistent with the possibility of statistical synergy as defined by Chou and Talalay (25), and a credible mechanism for this observation is described in the "Discussion." Taken together, the results of Fig. 3 demonstrate that microarray data are sufficient to generate verifiable hypotheses concerning agents that may increase the apoptotic and therapeutic potential of DNA damaging agents.

DISCUSSION

In HeLa cells, administration of 10 μM CPT results in apoptosis by 8 h. DNA damage induces ATM-mediated phosphorylation of p53 on serine 15 (26). To demonstrate that CPT addition was indeed inducing an effective DNA damage response, we examined p53 phosphorylation on serine 15 by Western analysis. Despite the widely reported loss of p53 stability mediated by human papillomavirus type E6 in HeLa (15, 27), we observed induction of genes that were previously noted to be transcribed via p53. These include *DTR* (*HB-EGF*), *DKK1, ATF3, GADD45 A&B*, *PMAIP1* (*Noxa*), and *ENC1* (*PIG10*).

Other moderately induced (<3-fold) p53-regulated genes include *IGFBP3*, *CDKN1A* (*p21 Waf1*), and *BTG2*. Others have found that CPT treatment results in p53 phosphorylation (28, 29) and reduced expression of *MDM2* (28), providing a plausible mechanism for our observation of possible p53-dependent effects. The induction of *p21* (*CDKN1A*) by CPT in HeLa is also consistent with previous observations in other cell systems (28). Our observation of strong GADD45 induction is also in accordance with a DNA damage-mediated p53 response. GADD45 protein may sterically hinder the proliferating cell nuclear antigen ring and thereby stall extension of S-phase replication forks (30). Consistent with this, we observe by fluorescence-activated cell sorting DNA content analysis a predominant S-phase arrest in nonapoptotic, CPT-treated HeLa cells by 24 h, occurring more rapidly at lower concentrations of the drug (data not shown). Still, other p53-inducible gene expression levels did not change significantly, and *PTEN* expression declined >3-fold. *RB1*, which is known to be repressed by p53 (31), declined in expression 8.7-fold. Because increased p53 protein level and phosphorylation on serine 15 is detectable by Western blot after treatment with CPT, these results are consistent with the induction of a partial or cell-specific p53 response mediated by CPT in HeLa cells.

Although p53-mediated increase in *Bax* (32, 33) or *PUMA* (*BBC3*; Ref. 34) level is sometimes regarded as a major mechanism for DNA damage-induced cell death, we did not find significant induction of these genes (Table 3*B*). However, a robust increase in the level of *PMAIP1* (*Noxa*) was detected, suggesting that this BH3-only protein may be involved in apoptosis initiation via its disruption of antiapoptotic Bcl-2 family members and subsequent stimulation of caspase-9

2100

Table 3 *Response of NF-κB-inducible and p53-responsive genes to camptothecin*

A. NF-κB-inducible genes			B. p53-responsive genes		
Gene symbol	False discovery rate	Fold Change	Gene symbol	False discovery rate	Fold Change
CCL20	1.39×10^{-3}	17.9	DTR	6.95×10^{-8}	8.0
IL8	2.65×10^{-3}	11.0	DKK1	6.95×10^{-8}	6.6
PTX3	1.08×10^{-2}	4.4	ATF3	6.95×10^{-8}	6.6
CXCL1	2.75×10^{-3}	3.8	GADD45B	2.37×10^{-6}	6.1
BDKRB1	5.28×10^{-3}	3.1	GADD45A	1.85×10^{-6}	5.0
NFKB2	6.37×10^{-2}	3.0	ENC1	8.31×10^{-6}	4.9
NFKBIA	1.47×10^{-4}	3.0	PMAIP1	7.40×10^{-7}	4.8
BIRC3	1.65×10^{-2}	2.7	IGFBP3	2.10×10^{-4}	2.6
IL6	7.63×10^{-5}	2.7	CDKN1A	1.31×10^{-3}	2.1
BLR1	1.32×10^{-1}	2.6	BTG2	4.05×10^{-3}	1.9
IL1A	2.36×10^{-2}	2.3	TAX1BP2	4.63×10^{-1}	1.6
WT1	2.47×10^{-1}	2.2	LRDD	5.74×10^{-1}	1.4
IRF1	7.71×10^{-4}	2.2	BBC3	4.74×10^{-1}	1.4
MYB	2.90×10^{-1}	2.2	PIG8	2.26×10^{-1}	1.3
TNFAIP3	1.21×10^{-3}	2.2	PCNA	2.09×10^{-1}	1.3
SOD2	2.76×10^{-1}	2.2	TNFRSF10B	1.95×10^{-1}	1.3
CCND1	4.69×10^{-3}	2.1	PTGES	2.41×10^{-1}	1.3
TNF	3.52×10^{-1}	2.0	PIGPC1	5.75×10^{-1}	1.2
HLA-E	2.25×10^{-3}	1.8	GAMT	8.11×10^{-1}	1.1
HLA-F	1.09×10^{-2}	1.7	PIG4 (GSAA)	8.98×10^{-1}	1.1
CSF1	2.98×10^{-2}	1.7	PIG11	9.98×10^{-1}	1.0
HLA-B	2.18×10^{-2}	1.6	PIG7	9.08×10^{-1}	−1.0
ICAM1	2.47×10^{-1}	1.6	PIG3	5.34×10^{-1}	−1.2
VCAM1	4.63×10^{-1}	1.5	LGALS7	8.19×10^{-1}	−1.3
HLA-G	5.25×10^{-2}	1.5	PRODH	6.24×10^{-1}	−1.5
MMP1	6.59×10^{-2}	1.5	BAX	2.41×10^{-1}	−1.6
TAP1	9.42×10^{-2}	1.5	MGC21654	1.15×10^{-1}	−1.8
HLA-C	3.26×10^{-2}	1.5	PIG5	1.10×10^{-1}	−1.8
TNFRSF6	1.38×10^{-1}	1.5	APAF1	8.80×10^{-1}	−1.9
IL12A	5.06×10^{-1}	1.4	MDM2	2.91×10^{-1}	−3.0
IL2RA	6.26×10^{-1}	1.4	PTEN	6.04×10^{-4}	−3.1
PSMB9	3.91×10^{-1}	1.4			
TNFSF6	6.28×10^{-1}	1.3			
PSMD2	7.83×10^{-2}	1.3			
HLA-A	2.42×10^{-1}	1.3			
NOS2A	7.71×10^{-1}	1.2			
BIRC2	4.86×10^{-1}	1.2			
PTGS2	7.53×10^{-1}	1.2			
LAMB2	5.65×10^{-1}	1.2			
CDKN2A	3.02×10^{-1}	1.2			
IL2	8.96×10^{-1}	1.2			
TRAF1	8.88×10^{-1}	1.1			
MYC	7.20×10^{-1}	1.1			
MMP9	9.12×10^{-1}	1.1			
SELE	9.65×10^{-1}	1.1			
MADCAM1	9.86×10^{-1}	1.0			
TP53	9.97×10^{-1}	−1.0			
IFNB1	9.78×10^{-1}	−1.0			
F3	7.82×10^{-1}	−1.1			
CSF2	8.85×10^{-1}	−1.2			
BIRC4	5.64×10^{-1}	−1.3			
TRAF2	2.46×10^{-1}	−1.4			
SERPINE1	2.72×10^{-1}	−1.5			
NFKB1	3.92×10^{-2}	−1.6			
BCL2A1	6.05×10^{-1}	−1.7			
ABCB1	5.26×10^{-1}	−1.7			

(35). Other potentially pro-apoptotic changes in the transcriptome include an increase in level of *GADD45* message, which may participate in c-Jun NH$_2$-terminal kinase activation (36) and an increase in *DKK1*, which disrupts survival signals mediated by the WNT signaling pathway (37). An approximate 2-fold increase in the levels of *tumor necrosis factor* (*TNF*)-α and one of its receptors, *TNFR2*, suggests that caspase-8 and Bid-mediated apoptosis could play an additional role in the induction of CPT-mediated apoptosis. TNF-α or similar ligands are likely to be active after CPT because significant up-regulation of *TNFAIP6* is observed.

In addition to apoptosis, the TNFR family of receptors also propagates proinflammatory and prosurvival signals mediated by NF-κB transactivation. Our finding of increase (4.5-fold) in the transcript level of *TNFRSF10D* (*TRAILRA*) implies that its corresponding protein may be transmitting signals via NF-κB without the caspase-recruiting TRADD domain that is characteristic of other TNFR family

members (38). Consistent with an increase in signaling via NF-κB and other inflammatory factors, we observe a 3-fold increase in expression of *NF-κB-2/RelB*, an almost 6-fold increase in *CD14*, a nearly 4-fold increase in *NFATC1*, and a 3.5-fold increase in *AOC1* (*VAP-1*). In addition, we detect increases in levels of NF-κB-inducible genes such as *BDKRB1*, *CXCL1*, *IL6*, *IL8*, *BIRC3* (*cIAP2*), and *PTX3*. Although NF-κB is known to be involved in responses to genotoxic stress (39), it is likely that this response attenuates the parallel apoptotic response, possibly allowing the cell time to repair the DNA or undergo a checkpoint-mediated arrest.

At least seven NF-κB-inducible genes have been implicated in a survival (or antiapoptotic) pathway (8). Of these, only the *BIRC3* (*c-IAP2*) gene is elevated (2.7-fold) after CPT treatment. Expression of BIRC3 has been shown to be sufficient to protect against etoposide-induced apoptosis in HT1080I cells (40). Several other genes implicated in NF-κB and/or apoptotic pathways are also up-regulated by
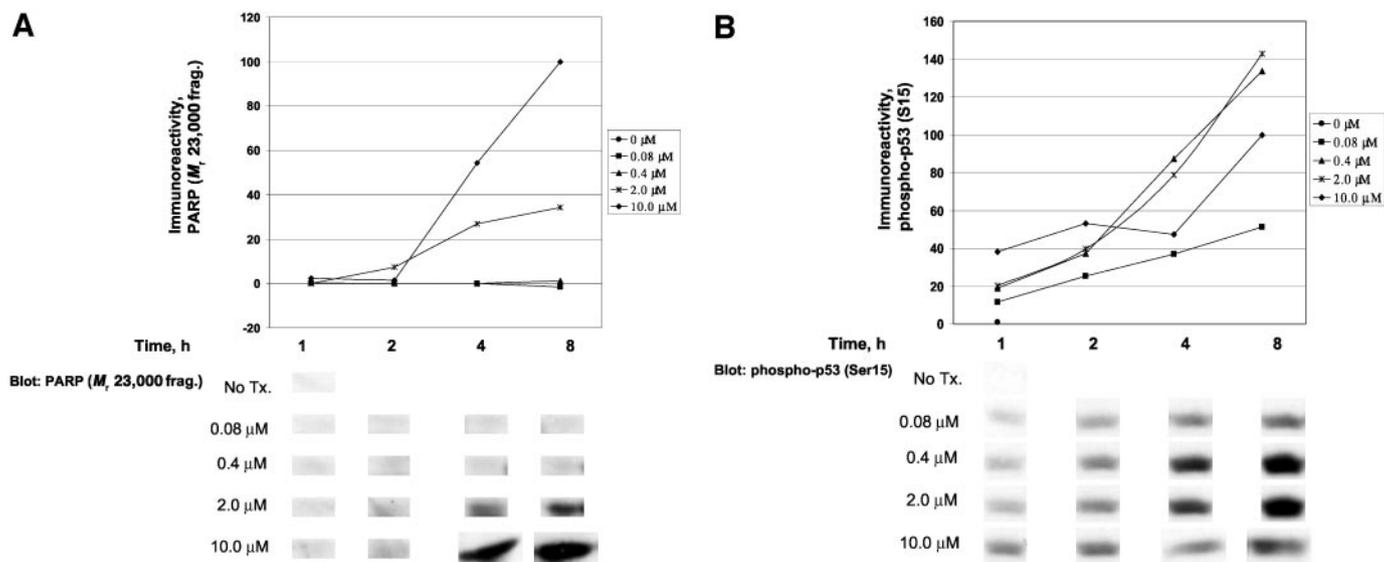
2101

Fig. 2. Camptothecin induces apoptosis and increased p53 activation in HeLa cells in representative single experiment depicting time and dose response of camptothecin-mediated apoptosis and p53 phosphorylation (serine 15) in HeLa cells. *A*, Western blot immunoreactivity and corresponding film images of caspase-specific, M_r 23,000 poly(ADP-ribose) polymerase (PARP) cleavage fragment; *B*, Western blot immunoreactivity and corresponding film images of active, serine 15-phosphorylated p53.

CPT exposure. These include NF-κB family member *NF-κB-2* (*p52/p100*) and the NF-κB inhibitor *NF-κB-IA* (*IκBα*). In addition, the *IRF1* and *TNFAIP3* genes are also up-regulated and reported to regulate apoptosis. Thus, our data demonstrate that up-regulation of a large number of genes controlled by NF-κB occurs in response to CPT exposure. Blockage of the NF-κB response using a dominant negative

form of the NF-κB inhibitor IkBα delivered with an adenovirus induces rapid apoptotic tumor regression in mice treated with the CPT derivative CPT-11 (9). This finding serves to validate the paradigm of examining CPT-responsive genes as potential targets for adjuvant therapy.

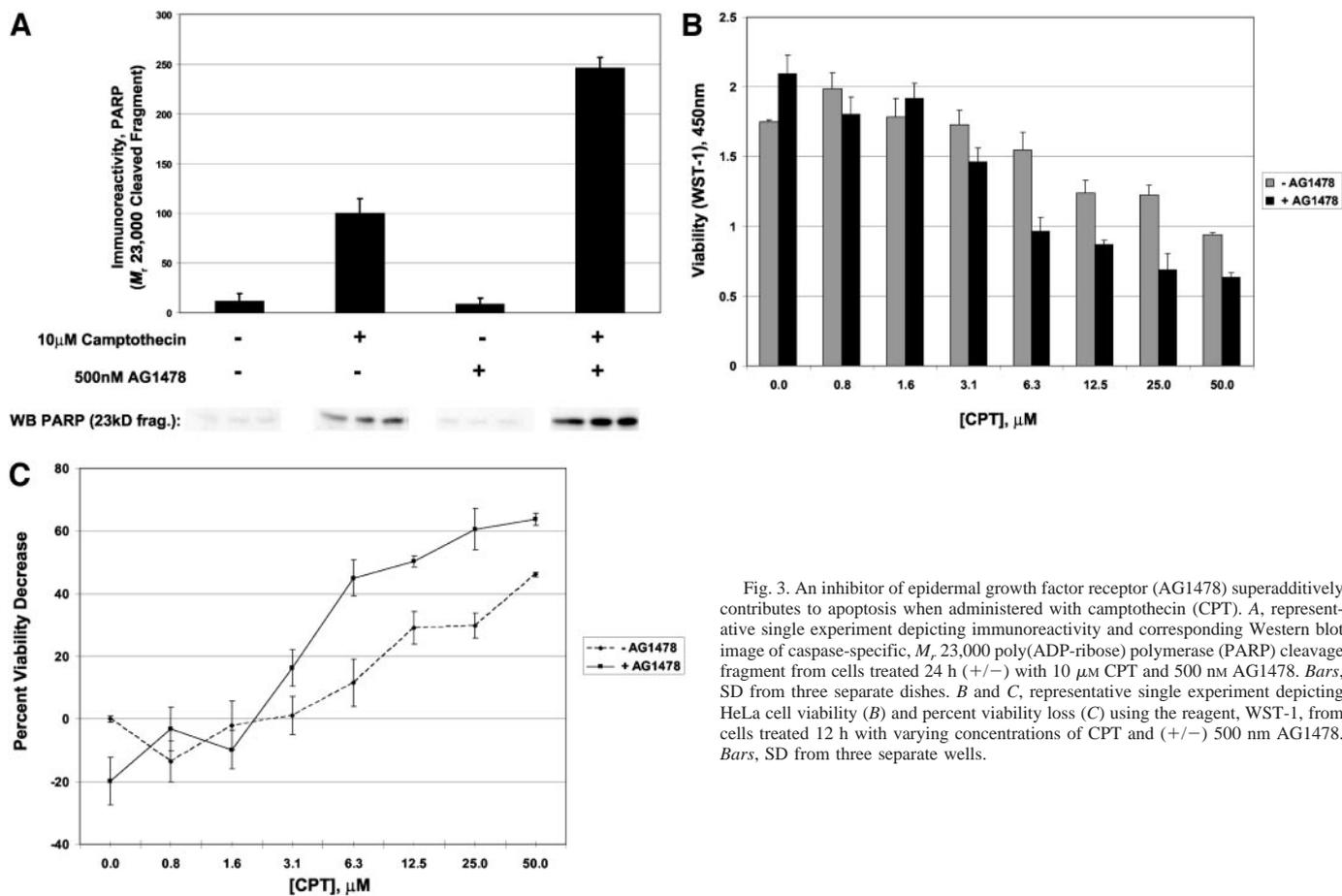In addition to p53 and NF-κB, other transcriptional responses to

Fig. 3. An inhibitor of epidermal growth factor receptor (AG1478) superadditively contributes to apoptosis when administered with camptothecin (CPT). *A*, representative single experiment depicting immunoreactivity and corresponding Western blot image of caspase-specific, M_r 23,000 poly(ADP-ribose) polymerase (PARP) cleavage fragment from cells treated 24 h (+/−) with 10 μM CPT and 500 nM AG1478. *Bars*, SD from three separate dishes. *B* and *C*, representative single experiment depicting HeLa cell viability (*B*) and percent viability loss (*C*) using the reagent, WST-1, from cells treated 12 h with varying concentrations of CPT and (+/−) 500 nM AG1478. *Bars*, SD from three separate wells.

2102

double-strand DNA breaks are likely to occur via MAFF, ATF3, LHX6, and GBX2 because their message levels are dramatically increased after 8 h of CPT treatment in HeLa cells. Interestingly, ATF3 is believed to repress transcription at the DNA binding elements of both cAMP-responsive element binding protein (41) and p53 (42), suggestive of a possible autoregulatory circuit involving p53. Additional complex regulatory networks may be engaged because potent induction of *DTR* (*HB-EGF*), dramatic decline in the level of *RasGAP*, and increases in the levels of immediate early genes *Fos1L* and *Jun* (*AP-1*) suggest that signaling through mitogen-activated protein kinase family pathways may be elevated. Prolonged mitogen-activated protein kinase activation, in contrast to the transient stimulations that produce cell cycle progression, could generate the opposite effect with cell cycle arrest and/or differentiation, as observed in PC12 (43, 44) and other epithelial cells (45). In agreement with this idea, we observe highly significant induction of *RIS1* (Table 1*C*), which correlates with Ras-mediated senescence but not DNA damage in fibroblasts (46).

Recently, it was demonstrated that a chromatin remodeling complex could replace H2A with an H2A variant called H2A.Z *in vitro* and *in vivo* (47), suggesting that the variant histones might be incorporated into damaged DNA. In addition, a homologue of *Saccharomyces cerevisiae Sir2*, *SIRT4*, is also highly elevated in expression after CPT treatment. Sir2 is a NAD-dependent histone deacetylase that silences transcription in telomeric regions (48). We have previously shown that posttranslational modifications of the nucleosome are required for repair of DNA damage caused by CPT (12).

If changes in the transcriptome after CPT treatment correlate with protein levels of the corresponding genes, the discovery of specific, CPT-inducible drug targets by microarray technology may enable adjunctive treatments that are beneficial to patients who are administered topo I inhibitors. Our finding of increased *DTR* (*HB-EGF*) level suggests that its gene product may activate its cognate receptor, ErbB1/EGFR, and generate downstream antiapoptotic signals via diverging pathways that could be Akt/PKB-dependent (49, 50) and/or independent (50, 51). This possible mechanism is consistent with a previous study from the Aaronson group, which demonstrated that DNA damage (mitomycin C) directed at certain cell lines causes p53-dependent induction of HB-EGF mRNA and protein level; this autocrine factor, in turn, seems to account for a significant fraction of Akt/PKB and mitogen-activated protein kinase activity induced by artificial p53 expression (50). Direct blockage of contrary EGFR-mediated survival signals might therefore increase the predominantly apoptotic effect of CPT in HeLa. To test this, we examined whether DTR (HB-EGF) is sufficient to protect HeLa cells against CPT-mediated apoptosis and determined that a highly specific inhibitor of the EGFR (AG1478) potentiates it. Currently, strategies to block growth and survival signals emanating from receptors of the ErbB family (Herceptin, C225, and Iressa) are under clinical investigation (16, 52). Similarly, the robust CPT-mediated increase in *SAT* transcript level led us to speculate that alteration of polyamine metabolism would be effective at increasing CPT-mediated apoptosis. The effect of polyamine depletion on apoptosis may differ dramatically depending on the cell type and nature of insult (53–55), and thus, additional experiments to elucidate whether pharmacological inhibition of synthesis—or catabolism—of spermine/spermidine via agents such as difluoromethylornithine may be justified. In addition, our finding of dramatic induction of certain variant histones (Fig. 1) prompts speculation that small molecule inhibitors of histone modification may prove effective in augmenting a response to topo I directed chemotherapy, perhaps by modulation of the proposed apoptotic histone code (56).

REFERENCES

1. Fisher DE. Apoptosis in cancer therapy: crossing the threshold. Cell 1994;78:539–42.
2. Singh D, Febbo PG, Ross K, et al. Gene expression correlates of clinical prostate cancer behavior. Cancer Cell 2002;1:203–9.
3. Schiller JH. Topotecan in small cell lung cancer. Semin Oncol 1997;24:S20-27–S20-33.
4. Fiorica J, Holloway R, Ndubisi B, et al. Phase II trial of topotecan and cisplatin in persistent or recurrent squamous and nonsquamous carcinomas of the cervix. Gynecol Oncol 2002;85:89–94.
5. Hertzberg RP, Caranfa MJ, Hecht SM. On the mechanism of topoisomerase I inhibition by camptothecin: evidence for binding to an enzyme-DNA complex. Biochemistry 1989;28:4629–38.
6. Kaufmann WK, Boyer JC, Estabrooks LL, Wilson SJ. Inhibition of replicon initiation in human cells following stabilization of topoisomerase-DNA cleavable complexes. Mol Cell Biol 1991;11:3711–8.
7. Zhou Y, Gwadry FG, Reinhold WC, et al. Transcriptional regulation of mitotic genes by camptothecin-induced DNA damage: microarray analysis of dose- and time-dependent effects. Cancer Res 2002;62:1688–95.
8. Orlowski RZ, Baldwin AS, Jr. NF-κB as a therapeutic target in cancer. Trends Mol Med 2002;8:385–9.
9. Wang CY, Cusack JC, Jr, Liu R, Baldwin AS, Jr. Control of inducible chemoresistance: enhanced anti-tumor therapy through increased apoptosis by inhibition of NF-κB. Nat Med 1999;5:412–7.
10. Benjamini Y, Hochberg Y. Controlling the false discovery rate: a practical and powerful approach to multiple testing. J R Royal Stat Soc 1995;57:289–300.
11. de Martin R, Schmid JA, Hofer-Warbinek R. The NF-κB/Rel family of transcription factors in oncogenic transformation and apoptosis. Mutat Res 1999;437:231–43.
12. Bird AW, Yu DY, Pray-Grant MG, et al. Acetylation of histone H4 by Esa1 is required for DNA double-strand break repair. Nature (Lond.) 2002;419:411–5.
13. Lowe SW, Schmitt EM, Smith SW, Osborne BA, Jacks T. p53 is required for radiation-induced apoptosis in mouse thymocytes. Nature (Lond.) 1993;362:847–9.
14. Lowe SW, Ruley HE, Jacks T, Housman DE. p53-dependent apoptosis modulates the cytotoxicity of anticancer agents. Cell 1993;74:957–67.
15. Kessis TD, Slebos RJ, Nelson WG, et al. Human papillomavirus 16 E6 expression disrupts the p53-mediated cellular response to DNA damage. Proc Natl Acad Sci USA 1993;90:3988–92.
16. Levitzki A. Protein kinase inhibitors as a therapeutic modality. Acc Chem Res 2003;36:462–9.
17. O'Shaughnessy JA, Demers LM, Jones SE, et al. α-Difluoromethylornithine as treatment for metastatic breast cancer patients. Clin Cancer Res 1999;5:3438–44.
18. de Bono JS, Rowinsky EK. Therapeutics targeting signal transduction for patients with colorectal carcinoma. Br Med Bull 2002;64:227–54.
19. Degterev A, Lugovskoy A, Cardone M, et al. Identification of small-molecule inhibitors of interaction between the BH3 domain and Bcl-xL. Nat Cell Biol 2001;3:173–82.
20. Haldar S, Jena N, Croce CM. Inactivation of Bcl-2 by phosphorylation. Proc Natl Acad Sci USA 1995;92:4507–11.
21. DiPaola RS, Aisner J. Overcoming bcl-2- and p53-mediated resistance in prostate cancer. Semin Oncol 1999;26:112–6.
22. Vigushin DM, Coombes RC. Histone deacetylase inhibitors in cancer treatment. Anticancer Drugs 2002;13:1–13.
23. Osherov N, Levitzki A. Epidermal-growth-factor-dependent activation of the src-family kinases. Eur J Biochem 1994;225:1047–53.
24. Daub H, Weiss FU, Wallasch C, Ullrich A. Role of transactivation of the EGF receptor in signalling by G-protein-coupled receptors. Nature (Lond.) 1996;379:557–60.
25. Chou TC, Talalay P. Quantitative analysis of dose-effect relationships: the combined effects of multiple drugs or enzyme inhibitors. Adv Enzyme Regul 1984;22:27–55.
26. Canman CE, Lim DS, Cimprich KA, et al. Activation of the ATM kinase by ionizing radiation and phosphorylation of p53. Science (Wash. DC) 1998;281:1677–9.
27. Scheffner M, Werness BA, Huibregtse JM, Levine AJ, Howley PM. The E6 oncoprotein encoded by human papillomavirus types 16 and 18 promotes the degradation of p53. Cell 1990;63:1129–36.
28. Ashcroft M, Taya Y, Vousden KH. Stress signals utilize multiple pathways to stabilize p53. Mol Cell Biol 2000;20:3224–33.
29. Xiao G, Chicas A, Olivier M, et al. A DNA damage signal is required for p53 to activate gadd45. Cancer Res 2000;60:1711–9.
30. Smith ML, Chen IT, Zhan Q, et al. Interaction of the p53-regulated protein Gadd45 with proliferating cell nuclear antigen. Science (Wash. DC) 1994;266:1376–80.
31. Shiio Y, Yamamoto T, Yamaguchi N. Negative regulation of Rb expression by the p53 gene product. Proc Natl Acad Sci USA 1992;89:5206–10.
32. Miyashita T, Reed JC. Tumor suppressor p53 is a direct transcriptional activator of the human bax gene. Cell 1995;80:293–9.
33. Yin C, Knudson CM, Korsmeyer SJ, Van Dyke T. Bax suppresses tumorigenesis and stimulates apoptosis *in vivo*. Nature (Lond.) 1997;385:637–40.
34. Jeffers JR, Parganas E, Lee Y, et al. Puma is an essential mediator of p53-dependent and -independent apoptotic pathways. Cancer Cell 2003;4:321–8.

35. Oda E, Ohki R, Murasawa H, et al. Noxa, a BH3-only member of the Bcl-2 family and candidate mediator of p53-induced apoptosis. Science (Wash. DC) 2000;288: 1053–8.

36. Takekawa M, Saito H. A family of stress-inducible GADD45-like proteins mediate activation of the stress-responsive MTK1/MEKK4 MAPKKK. Cell 1998;95:521–30.

37. Grotewold L, Ruther U. The Wnt antagonist Dickkopf-1 is regulated by Bmp signaling and c-Jun and modulates programmed cell death. EMBO J 2002;21:966–75.

38. Degli-Esposti MA, Dougall WC, Smolak PJ, Waugh JY, Smith CA, Goodwin RG. The novel receptor TRAIL-R4 induces NF-κB and protects against TRAIL-mediated apoptosis, yet retains an incomplete death domain. Immunity 1997;7:813–20.

39. Mayo MW, Baldwin AS. The transcription factor NF-κB: control of oncogenesis and cancer therapy resistance. Biochim Biophys Acta 2000;1470:M55–62.

40. Wang CY, Mayo MW, Korneluk RG, Goeddel DV, Baldwin AS, Jr. NF-κB antiapoptosis: induction of TRAF1 and TRAF2 and c-IAP1 and c-IAP2 to suppress caspase-8 activation. Science (Wash. DC) 1998;281:1680–3.

41. Low KG, Chu HM, Schwartz PM, Daniels GM, Melner MH, Comb MJ. Novel interactions between human T-cell leukemia virus type I Tax and activating transcription factor 3 at a cyclic AMP-responsive element. Mol Cell Biol 1994;14: 4958–74.

42. Yan C, Wang H, Boyd DD. ATF3 represses 72-kDa type IV collagenase (MMP-2) expression by antagonizing p53-dependent trans-activation of the collagenase promoter. J Biol Chem 2002;277:10804–12.

43. Marshall CJ. Specificity of receptor tyrosine kinase signaling: transient versus sustained extracellular signal-regulated kinase activation. Cell 1995;80:179–85.

44. Vaudry D, Stork PJ, Lazarovici P, Eiden LE. Signaling pathways for PC12 cell differentiation: making the right connections. Science (Wash. DC) 2002;296:1648–9.

45. Kim J, Adam RM, Freeman MR. Activation of the Erk mitogen-activated protein kinase pathway stimulates neuroendocrine differentiation in LNCaP cells independently of cell cycle withdrawal and STAT3 phosphorylation. Cancer Res 2002;62: 1549–54.

46. Barradas M, Gonos ES, Zebedee Z, et al. Identification of a candidate tumor-suppressor gene specifically activated during Ras-induced senescence. Exp Cell Res 2002;273:127–37.

47. Mizuguchi G, Shen X, Landry J, Wu WH, Sen S, Wu C. ATP-driven exchange of histone H2AZ variant catalyzed by SWR1 chromatin remodeling complex. Science (Wash. DC) 2003;303:343–8.

48. Imai S, Armstrong CM, Kaeberlein M, Guarente L. Transcriptional silencing and longevity protein Sir2 is an NAD-dependent histone deacetylase. Nature (Lond.) 2000;403:795–800.

49. Kulik G, Klippel A, Weber MJ. Antiapoptotic signalling by the insulin-like growth factor I receptor, phosphatidylinositol 3-kinase, and Akt. Mol Cell Biol 1997;17: 1595–1606.

50. Fang L, Li G, Liu G, Lee SW, Aaronson SA. p53 induction of heparin-binding EGF-like growth factor counteracts p53 growth suppression through activation of MAPK and PI3K/Akt signaling cascades. EMBO J 2001;20:1931–9.

51. Carson JP, Kulik G, Weber MJ. Antiapoptotic signaling in LNCaP prostate cancer cells: a survival signaling pathway independent of phosphatidylinositol 3′-kinase and Akt/protein kinase B. Cancer Res 1999;59:1449–53.

52. Cohen MH, Williams GA, Sridhara R, Chen G, Pazdur R. FDA drug approval summary: gefitinib (ZD1839) (Iressa) tablets. Oncologist 2003;8:303–6.

53. Packham G, Cleveland JL. Ornithine decarboxylase is a mediator of c-Myc-induced apoptosis. Mol Cell Biol 1994;14:5741–7.

54. Stefanelli C, Pignatti C, Tantini B, et al. Effect of polyamine depletion on caspase activation: a study with spermine synthase-deficient cells. Biochem J 2001;355:199–206.

55. Yuan Q, Ray RM, Johnson LR. Polyamine depletion prevents camptothecin-induced apoptosis by inhibiting the release of cytochrome c. Am J Physiol Cell Physiol 2002;282:C1290–7.

56. Cheung WL, Ajiro K, Samejima K, et al. Apoptotic phosphorylation of histone H2B is mediated by mammalian sterile twenty kinase. Cell 2003;113:507–17.

Pharmacogenomic Identification of Targets for Adjuvant Therapy with the Topoisomerase Poison Camptothecin

Jonathan P. Carson, Nianyi Zhang, Garrett M. Frampton, et al.

Updated version	Access the most recent version of this article at: http://cancerres.aacrjournals.org/content/64/6/2096

Cited articles	This article cites 55 articles, 22 of which you can access for free at: http://cancerres.aacrjournals.org/content/64/6/2096.full#ref-list-1
Citing articles	This article has been cited by 5 HighWire-hosted articles. Access the articles at: http://cancerres.aacrjournals.org/content/64/6/2096.full#related-urls

E-mail alerts	Sign up to receive free email-alerts related to this article or journal.
Reprints and Subscriptions	To order reprints of this article or to subscribe to the journal, contact the AACR Publications Department at pubs@aacr.org.
Permissions	To request permission to re-use all or part of this article, use this link http://cancerres.aacrjournals.org/content/64/6/2096. Click on "Request Permissions" which will take you to the Copyright Clearance Center's (CCC) Rightslink site.